International Journal of Advanced Interdisciplinary Sciences

Vol.1, Issue.1, August 2021,112-126

Investigation of Structural and Dielectric Properties of α-Fe_2O_3 /Mn_2O_3 Nanostructures Prepared by DNA Assisted Precipitation Method

Smitha S[a*], Anu Krishna P G[a], Nisha J Tharayil[a]

[a] Department of Physics, S.N College for Women (affiliated to University of Kerala), Kollam, Kerala-691001.

*Corresponding author: smitha6feros@gmail.com

Abstract

DNA (Deoxyribonucleic acid) assisted chemical co precipitation method was used to prepare mixed transition metal oxide of α -Fe_2O_3/Mn_2O_3 nanostructures with various concentrations. For the preparation, iron (III) chloride and manganese (II) chloride were used as precursors. This study investigated the influence of Mn concentration on the characteristics of prepared mixed oxide nanostructures. The compositional, structural and morphological characterizations of the samples were done by Energy Dispersive X-Ray Spectroscopy (EDS), X-Ray Diffraction (XRD), Fourier Transform Infrared Spectroscopy (FTIR) and Scanning Electron Microscope (SEM) analysis. EDS confirms the composition and stoichiometry of Fe, Mn and O in the samples. XRD data indicate the presence of rhombohedral phase of hematite and cubic phase of Mn_2O_3 in the prepared samples. In FTIR, bands appearing below 600 cm^{-1} confirms metal oxide bonds. SEM micrographs clearly show the reduction in particle size and densification of materials caused by cation addition. The variations of dielectric constant, ac conductivity, dielectric loss etc. of the nanostructures at room temperature were studied as a function of Mn concentration and frequency.

Key words: Mixed nanostructures, DNA, Dielectric properties.

Article History: Received 7 July 2021; Revised 7 August 2021; Accepted 20 August 2021; Published 31 August 2021.

1. Introduction

Metal oxide nanoparticles and related nanocomposites materials, which have emerged as 21st century materials with potentially intriguing characteristics, have been extensively investigated in a variety of scientific disciplines [1]. Mixed nanostructures can be prepared from any combination of materials in order to produce improved electrical and thermal conductivity [2]**,** enhanced optical and catalytic properties [3], excellent dielectric and magnetic properties [4] etc. By introducing one transition metal oxide in to another can produce mixed transition metal oxide nanostructures with favorable electrical and magnetic properties in a controllable fashion. Comprehending the complete characteristics of binary metal oxide is a challenging task because of the system complexity [5]. Transition metal oxides occupy a unique place in mixed oxide nanostructures designing and fabrication due to the existence of partly filled 3d electrons, which exhibit a range of unusual properties. The combination of two such transition metal oxides offer a viable path to achieving the desired property for specific applications.

In this proposed work, a seldom researched combination of two transition metal oxide α-Fe_2O_3 and Mn_2O_3 were selected for in-depth investigation. Among the polymorphs of iron (III) oxide (α-Fe_2O_3, β- Fe_2O_3, γ- Fe_2O_3, ε-Fe_2O_3), α-Fe_2O_3 is the most stable polymorph under ambient condition. Dielectric and magnetic properties of iron oxide nanoparticles seeking attention among material scientists to exploit the intrinsic properties of nanoparticles in biomedical field [6-8], magnetic data storage devices [9], catalysis [10-12], photochemical water splitting [13], lithium-ion batteries[14], spintronics [15] etc. As a combinatory oxide to enhance the dielectric properties of hematite, Mn_2O_3 were selected for mixed oxide nanostructure synthesis. Previously reported articles of Youn et al. finds proper conditioning of the Mn content in Fe-Mn alloys to improve its visibility on MR angiography [16].Thus proper tuning of magnetic and dielectric properties of these nanostructures can be achieved by controlled addition of Mn to hematite matrix. In this work it has been noted that the properties of prepared binary transition metal oxide nanocomposites are extremely sensitive to composition and structure. A comprehensive study of this relationship will lead to the better understanding of the multifunctional behavior of the nanocomposites.

Several synthesis techniques are available for the synthesis of mixed metal oxide nanocomposites with controllable particle size, shape and properties. These methods have shown several advantages and limitations. Some of the popular routes for preparation of mixed oxides are co precipitation [17], sol-gel method [18], combustion method [19], microwave-assisted synthesis

[20], chemical reduction [21] etc. Co precipitation (wet precipitation) is the simple and cost-effective method, widely used for magnetic oxide synthesis. Here, oxo-hydroxides of the metals are precipitated from their aqueous metal salts solution by using strong basic solution as precipitating agent. The hydroxide is washed, dried, and calcined to get the metal oxide. An advantage of this method is that by adjusting the pH and ionic strength of the precipitating medium, the mean size of the particle can be controlled which helpful in the generation of size dependent magnetic properties in nanoparticles [22].

Herein, we present the structural and dielectric properties of mixed transition metal oxide of α-Fe_2O_3 /Mn_2O_3 nanostructures with different Mn concentration prepared by DNA assisted chemical co precipitation method. Usually, nanoparticles are aggregate due to its high surface energy and magnetization. To prevent agglomeration and to enhance stability DNA template for nanocomposite fabrication has been opted. The major aim of the study is to gain insight into the effects of Mn substitution in modifying the characteristics of hematite for specific applications.

2. Materials and methods

Mixed transition metal oxide of α-Fe_2O_3 /Mn_2O_3 were prepared by DNA assisted chemical co-precipitation method by using iron (III) chloride and manganese (II) chloride as cationic precursors. Sodium hydroxide solution, an anionic precursor is used to adjust the pH of the solution to enable precipitation. DNA acts as a good stabilizing agent as well as a template for nano particles. By varying molarity of manganese (II) chloride (as 0.025M, 0.05M and 0.1M) three samples of nanocomposites were prepared. In all these samples molarity of Iron (III) chloride kept fixed (0.1M). It is observed that variation of molarity of any one of the precursors differently affect over all properties of the nanocomposites. After completing 5 hrs of reaction hydroxide precipitate obtained was washed with alcohol and distilled water several times then dried and thoroughly ground. The fine powder was heated at a temperature obtained from TGA/DTA, at 600^0C for 3hrs, to obtain required Iron-manganese oxide nanocomposites. In the present work the three different samples were named as FM1 (0.025M $MnCl_2$ & 0.1M $FeCl_3$), FM2 (0.05M $MnCl_2$ & 0.1M $FeCl_3$) and FM3 (0.1M $MnCl_2$ & 0.1M $FeCl_3$) throughout in this work.

2.1. Characterization of the samples

Energy dispersive X-ray analysis (EDS) of the samples was done using CARL ZEISS EVO 18 SEM with EDS instrument. The XRD measurements of the prepared samples were done using XPERT-PRO model X-ray diffractometer using CuKα radiation of wavelength λ=1.5406A^0 at

40KV and 100mA. The FTIR studies of all the samples were carried out in a Perkin-Elmer FTIR spectrometer. Morphological analysis was carried out using scanning electron microscope (JEOL Model JSM - 6390LV). The dielectric measurements are done using Hioki 3532-50 LCR Hit ESTER in the frequency range 50 Hz to 5MHz at the room temperature range. The magnetic properties of the nanoparticles were performed at room temperature (300K) using a cryogen-free vibrating sample magnetometer (Cryogenics Ltd, UK) at an applied magnetic field of −2 to 2 T.

3. Results and Discussion

3.1. Compositional analysis using Energy Dispersive X-Ray (EDS) Analysis

The elemental compositions of the samples were confirmed by EDS analysis and peaks obtained are shown in the **Figure 1.** The EDS spectrum indicates the presence of Fe, Mn and O in the sample.

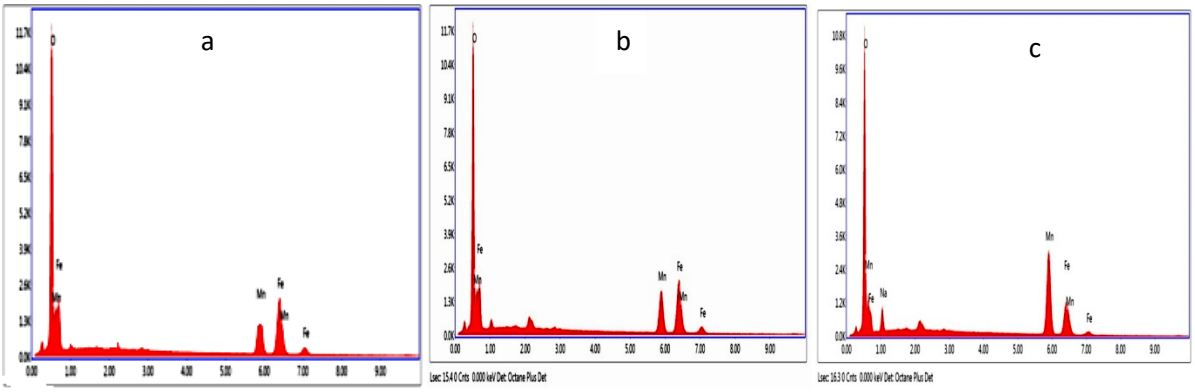

Figure 1. EDS spectrum of a) FM1, b) FM2 and c) FM3

3.2. Structural analysis

The XRD patterns of three different α-Fe_2O_3 /Mn_2O_3nanostructures were shown in **Figure 2**. In FM1and FM2 samples intensity of α-Fe_2O_3 phase is dominated. XRD patterns of these two samples show two prominent peaks from the planes (104) and (110) along with weak intense peaks from (116),(024),(012),(300),(125),(113).The presence of these peaks revealed the rhombohedral phase of hematite in two samples and no evidence of the presence of Mn_2O_3 phase and match with JCPDS Card No.001-1053 .This indicates that Mn ions substituted Fe sites without affecting crystal structure of the host. But in FM3 the phase separation between α-Fe_2O_3 and Mn_2O_3 is clearly visible and the formation of the mixed oxide nanostructures was confirmed. The most intense diffraction peak from (104) at $2\theta=33^0$ confirms the formation of both phases in the sample.

Compared with FM1and FM2 intensity of other peaks of hematite phase is slightly reduced due to the more addition of manganese oxide phase in FM3. The intense peak from the planes (104), (440) and other peaks from (211), (400), (522),(322) confirms the cubic phase of $Mn_2O_3$with JCPDS Card No.041-1442.The XRD analysis of above samples indicates the formation of α-Fe_2O_3 /Mn_2O_3 nanostructures with pure crystalline nature.

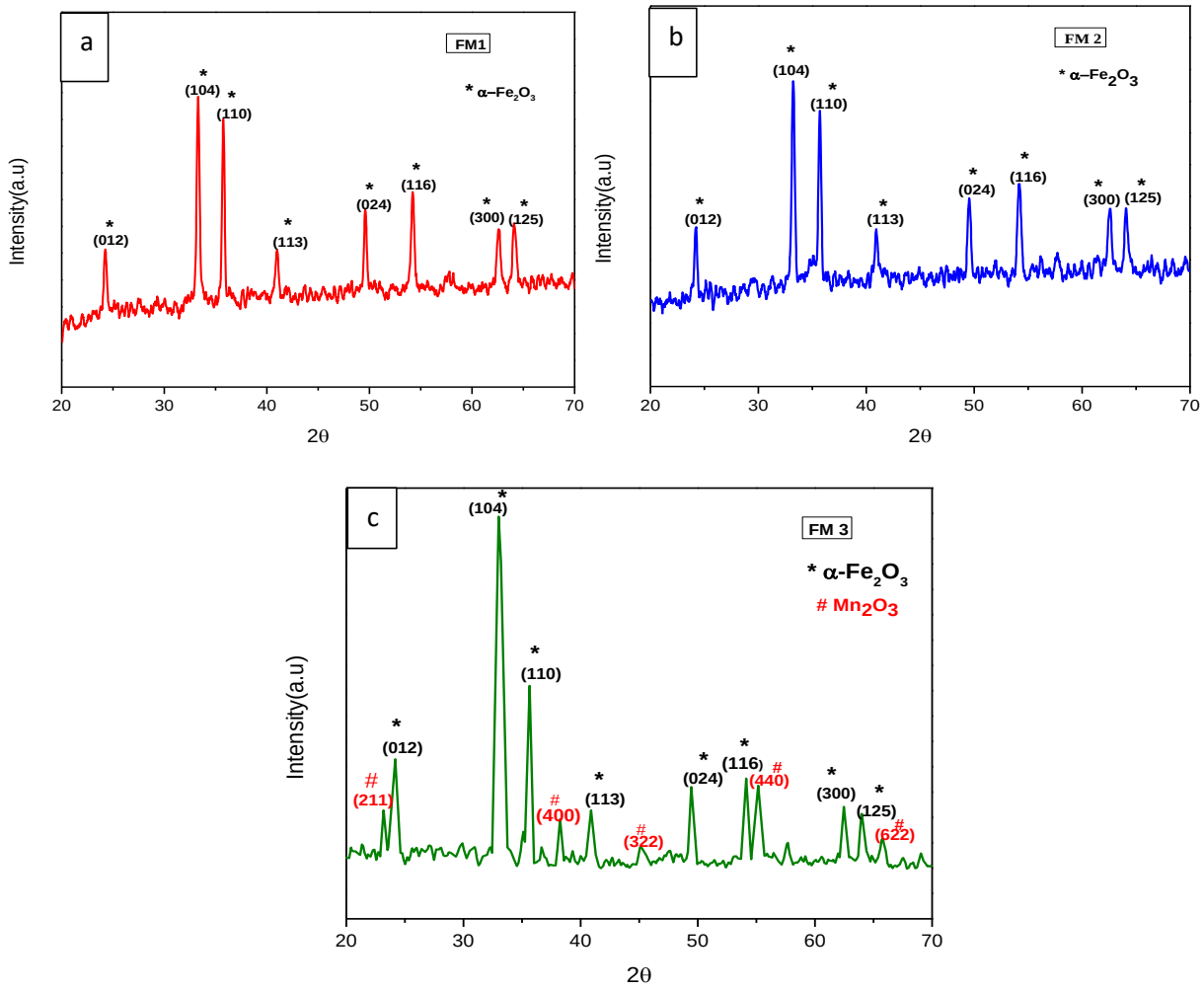

Figure 2. XRD pattern of a) FM1, b) FM2 and c) FM3

The crystallite size of the particles was calculated using Debye Scherrer's formula, D=Kλ/βcosθ. Where β = full width half maximum (FWHM), K = grain shape dependent constant (0.9), λ= wavelength of incident beam, θ = Bragg Reflection angle in degree. The obtained sizes of the particles were 39.16 nm, 31.85 nm and 27.74 nm for FM1, FM2 and FM3 respectively. Thus

particle size of the nanostructures has been found to be regulated by the application of manganese. The incorporation of manganese disturbs the grain growth due to strain and limits grain size. In current synthesis method, there are two possibilities of product formation such as ferrites formation and binary metal oxide composites. Here 5 hours of stirring without thermal treatment, oxidation states of Fe and Mn, pH and the presence of biosurfactant favors the formation of mixed metal oxide composites. XRD analysis confirms the formation of well-crystallized α-Fe_2O_3 /Mn_2O_3 nanostructures

3.3. Fourier transform infrared spectroscopy (FTIR)

FTIR spectrums of the synthesized nanostructures were studied between 400 - 4000 cm^{-1} shown in **Figure 3.** Peaks appearing below 600 cm^{-1} are due to metal oxide bonds. The band around 517 cm^{-1} and 428 cm^{-1} is attributed to the Fe–O stretching and bending vibration mode of α-Fe_2O_3 respectively. In FM3, the intensity of the peak at 517 cm^{-1} is reduced due to the formation of mixed oxide nanostructures. The broad peaks around 3300-3405cm^{-1} indicates the presence of stretching vibration of intermolecular hydrogen bond (O-H) bond. The peak at 2364 cm^{-1} can be assigned to C-O vibration [23]. The weak band near 1600 cm^{-1} is assigned to H–O–H bending vibrations mode. The appearance of such peak is representative of adsorbed water molecules on the external surface of the samples.

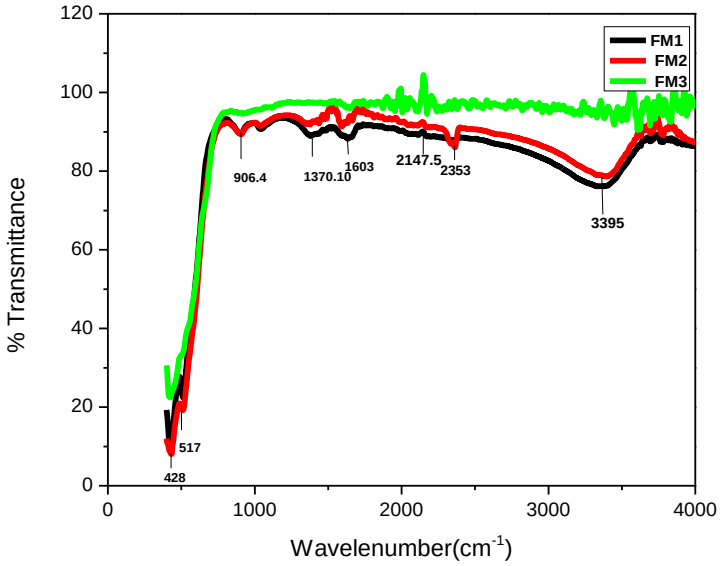

Figure 3. FTIR spectrums of FM1, FM2 and FM3

3.4. Scanning electron microscopy (SEM)

SEM image of three different samples, which was taken at 20 kV accelerating voltage and 3500 magnification is shown in **Figure 4**. It is clear from the images that surface morphology of the samples depends strongly on cation (Mn ion) addition. Decrease in particle size by cation addition can be clearly detectable from the images. The shapes of the particles were non uniform and distributed heterogeneously with more porosity. The image shows that the sample is well densified due to the addition of manganese.

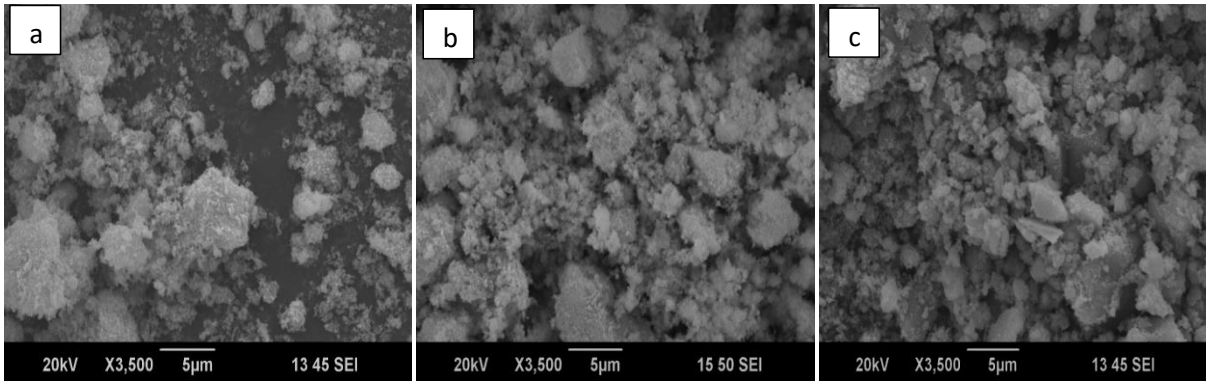

Figure 4. SEM images of a) FM1, b) FM2 and c) FM3

3.5. Dielectric studies

The dielectric properties of the synthesized nanostructures as a function of frequency and composition are explored in depth at room temperature.

3.5.1 Frequency dependence of dielectric constant (ε') and dielectric loss (ε'')

The frequency (log f) dependence of the real (**ε'**) and imaginary (**ε''**) parts of the dielectric constant in the frequency range 50HZ–5MHz at room temperature are shown in **Figure 5a and 5b**The variation of dielectric constant **ε'** with frequencies show normal behavior at room temperature. That is the value of dielectric constant is higher at lower frequencies and decreases exponentially with increasing frequency and then reaches a constant value which shows that it is independent of frequency at higher values. This behavior is observed in ferrites and is mainly attributed to the Maxwell-Wagner type polarization [24] and Koop's phenomenological model [25]. This arises due to the presence of large number of conducting grain separated by grain boundaries. It is reported that in hematite electron hopping follows a small polaron hopping mechanism between nearest Fe^{2+}/Fe^{3+} atoms [26]. In FM1and FM2 the concentration of iron ions is greater which increases

charge carriers which accumulate at the grain boundary at low frequency which increases dielectric property. The exponential decrease in dielectric constant with frequencies is due to dielectric relaxation or delay in polarization due to the field variation. But comparing three samples, dielectric constant is greater for FM1. The dielectric behavior of these nanostructures resembles with certain spinal ferrites. The theory behind the formation of dielectric polarization and electric conduction are the same. The imaginary part of permittivity, **ε''** represents the energy loss measurements during polarization process by dynamic electric field. Dielectric loss ε" shows a decrease with frequency. Decrease of dielectric loss with frequency indicates the maximum efficiency of the material for electronic and communication application.

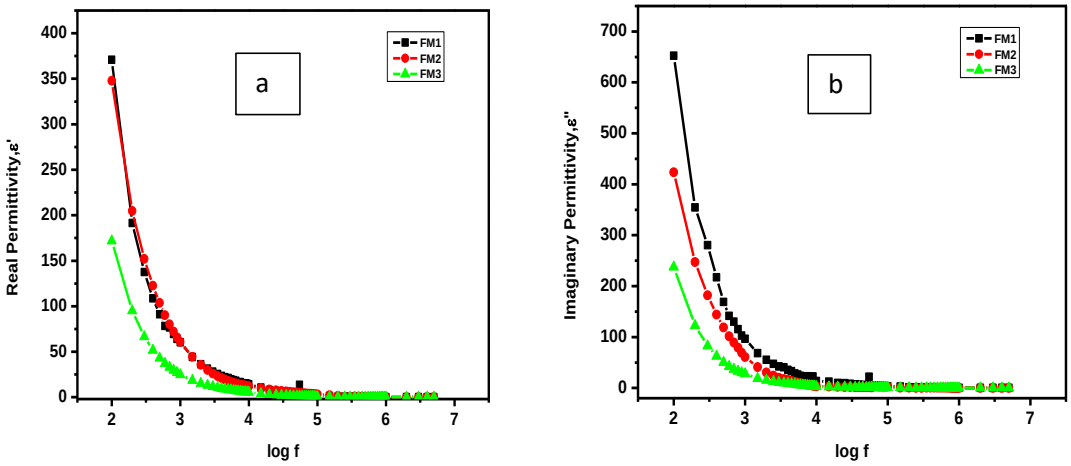

Figure 5. Variation of real and imaginary permittivity with frequency at different concentration shown in (i) a and (ii) b

3.5.2 Frequency dependence of loss tangent and tan δ

Loss tangent of dielectric materials has as much important in determining efficiency of the material in electronic engineering. It measures the loss of energy in the sample when external electric field applied in to it. Loss tangent as a function of frequency at room temperature is as in **Figure 6,** and the loss tangent shows an anomalous behavior. Variation of Loss tangent with Mn concentration is as shown in **Figure 7.**The origin of this anomalous behavior is observed due to the presence of Mn ions in the sample. The loss tangent curves show dielectric relaxation peaks at certain frequency at room temperature, a maximum of loss may be observed as a peak. Here loss tangent peaks of α-Fe_2O_3/Mn_2O_3 nanostructures are mainly depend on the composition. A small variation

in composition is found to be affecting the loss tangent peaks. Relaxation peaks in this heterogeneous material could be clearly explained with Rezlescu model [27]. This model explains peaking behavior of loss tangent curve, a resonance peak occurs when hopping frequency of two opposite charge carriers (p-type and n-type) becomes equal to the frequency of alternating electric field. At resonance $2\pi f_m \tau = 1$, where f_m is the maximum frequency and τ is the relaxation time of hopping mechanism. It is also note that tan δ maximum occurs at frequency 450 KHz, 500 KHz, 2000 KHz for FM1, FM2 and FM3respectively.A right shift of relaxation peak occurs in the case of FM2 compared to FM1 and FM3. Right shift of relaxation peak indicates larger concentration of Fe^{3+} carriers. The left ward shift of peak in FM3 is due to the larger concentration of p-type (Mn^{3+}) carriers or smaller concentration of n-type (Fe^{3+}) carriers.

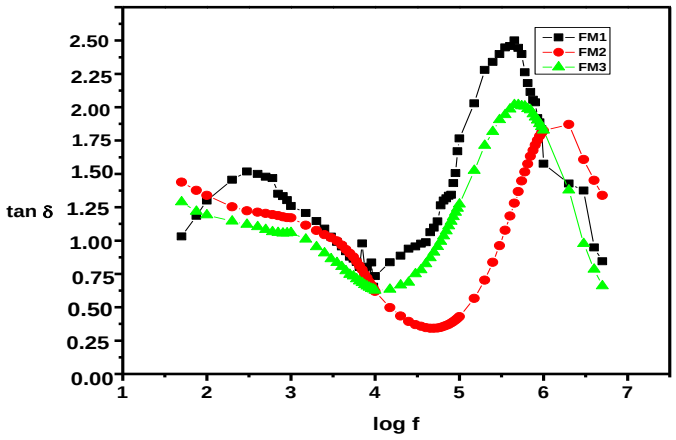

Figure 6. Variation of tan δ with frequency at different concentration

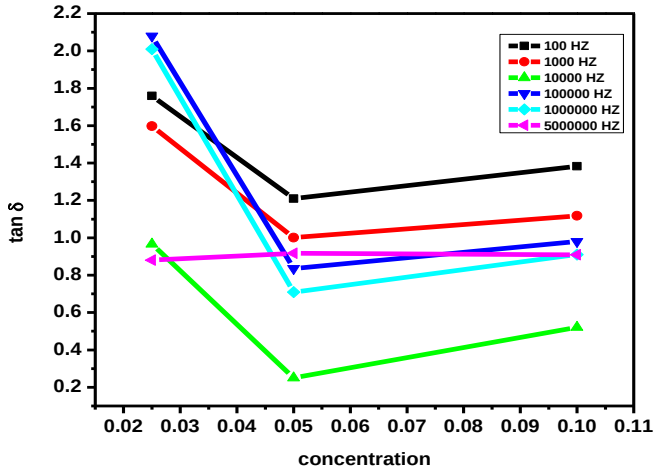

Figure 7. variation of tan δ with concentration at different frequencies

3.5.3 Frequency dependence of AC conductivity, σ_{ac}

At lower frequencies ac conductivity seems to be nearly frequency independent for all nanostructures. Frequency dependent ac conductivity of the materials shows an increase in higher frequency region as in **Figure.8.** At higher frequency of the external field, the conductive grains become more active than grain boundary, this promotes the hopping conduction. In these nanostructures two types of conduction mechanisms possible electron hopping (Fe^{2+}/Fe^{3+}) and hole hopping (Mn^{2+}/Mn^{3+}).It is observed that ac conductivity decreases due to Mn addition in α-Fe_2O_3 matrix.

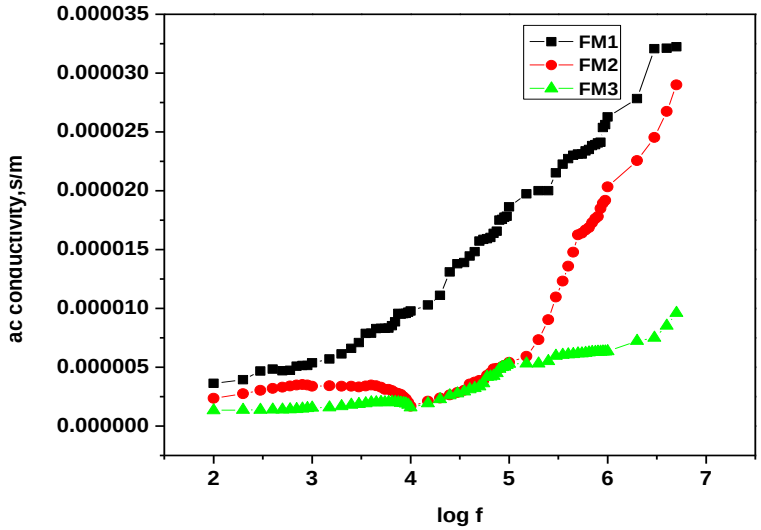

Figure 8. Variation of ac conductivity of nanostructures with frequency at different concentration

3.5.4 Composition dependence of ε', ε'' and tan δ

The compositional dependence of real and imaginary part of dielectric constant for three samples at different frequencies as presented in **Figure 9**. Present work reveals that there is large dispersion in dielectric constant and dielectric loss with frequency and Mn content in the nanostructures. Dielectric constant vs. concentration curve shows sharp decrease in the value of ε' and ε" for FM3 samples at low frequency. It is due to the fact that FM1and FM2 samples are found to be in rhombohedral phase of hematite by XRD analysis. It can be observed that addition of small content of Mn ion replaces Fe ions in hematite matrix and increases p-type low mobile carries which in fact slightly decreases the n-type Carriers of hematite. But in the case of FM3 due to higher concentration of Mn favors the formation of two phased α-Fe_2O_3/Mn_2O_3 nanostructure. The presence of two phases at the grain boundary decreases the value of dielectric constant. It is also

noted that the grain size reduction and porosity created by the addition other phases causes in homogeneity in nanostructures which is also a factor for affecting the value of dielectric constant. The grain size reduction caused by Mn addition is also a factor for the decrement of dielectric constant. That is polarization dependent dielectric properties decreases with smaller crystalline size nanoparticles.

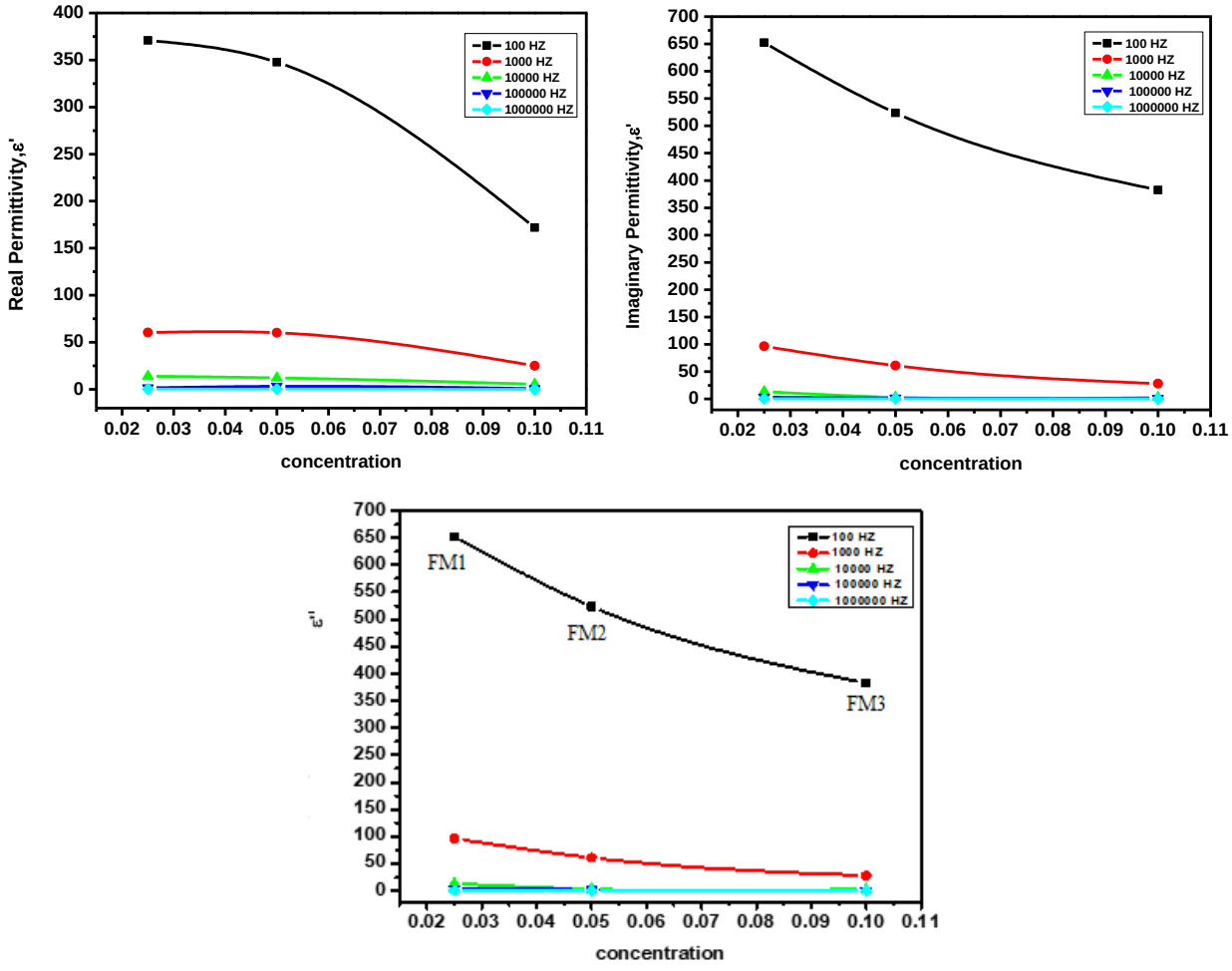

Figure 9. Variation of dielectric constant ε' and ε" with concentration at different frequencies

The dielectric loss tangent determines the quality of a sample. Quality of a sample is expressed in Q-factor; here it is the reciprocal of tan δ. All the samples show maximum loss at higher frequencies as shown in **Figure 10**. Among the three samples FM1 shows high loss compared to other two. Q-factor value is highest for FM2. Presence of two phases in FM3 slightly increases loss.

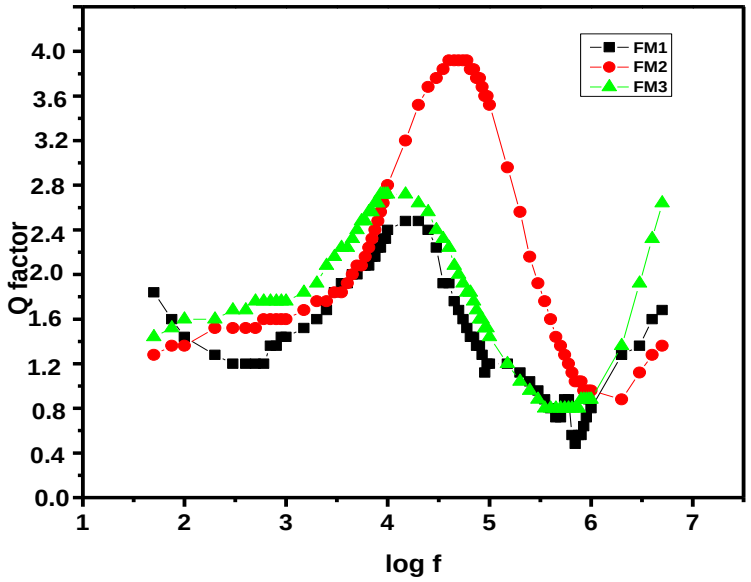

Figure 10. Variation of Q factor with frequencies at different concentration

4. Conclusions

Mixed transition metal oxide of α-Fe_2O_3 /Mn_2O_3 nanostructures with different Mn concentration were successfully prepared by DNA assisted chemical co precipitation method. The XRD studies revealed that prepared nanostructure consists of both phases - rhombohedral phase of hematite and cubic phase of Mn_2O_3. Manganese has a substantial influence on the surface morphology of nanostructures, indicating that the sample is highly densified as a result of manganese addition. Dielectric studies revealed that dielectric properties increase as the particle size increases and decreases with Mn substitution. It may be due to the large particles containing more ferrous ions than the small particles, and becoming more conductive. The low value of loss tangent observed for the composite FM2 make them a suitable candidate for dielectric applications.

Acknowledgements: The authors are also pleased to acknowledge Cliff, Kariavattom and STIC, Cochin.

Funding source: No external funding for the present Research work.

Conflict of Interest: There is no conflict of interest.

References

[1] P. H. C. Camargo, K. G. Satyanarayana, F. Wypych, Nanocomposites: synthesis, structure, properties and new application opportunities, Materials Research, 12 (2009) 1-39.

[2] W. E. Jones, J. Chiguma, E. Johnson, A. Pachamuthu, D. Santos, Electrically and thermally conducting nanocomposites for electronic applications, Materials (Basel). (2010) 1478–1496**.**

[3] S. Usharani, V. Rajendran, Optical, magnetic properties and visible light photocatalytic activity of CeO_2/SnO_2 nanocomposites, Engineering Science and Technology, 19 (2016) 2088-2093.

[4] R. Gholipur, A. Bahari, Effect of electric field on the dielectric and magnetic properties of random nanocomposites, Materials and Design, 94 (2016) 139-147.

[5] C. Yuan, H. B. Wu, Y. Xie, X. W. Lou, Mixed transition-metal oxides: Design, synthesis, and energy-related applications, Angewandte Chemie, 53 (2014) 1488–1504.

[6] W. Wu, Z. Wu, T. Yu, C. Jiang, and W.S. Kim, Recent progress on magnetic iron oxide nanoparticles: synthesis, surface functional strategies and biomedical applications, Science and Technology of Advanced Materials.16 (2015) 023501.

[7] K. McNamara, S.A.M. Tofail, Nanoparticles in biomedical applications, Advances in Physics: X (2017) 54-88.

[8] P. Sangaiya, R. Jayaprakash. A Review on Iron Oxide Nanoparticles and Their Biomedical Applications. Journal of Superconductivity and Novel Magnetism. 31 (2018) 10948-018-4841-2.

[9] T.J. Zhou, K.M. Cher, P. W. Lwin, J.F. Hu, Energy barrier measurement and optimization in exchange coupled Fe Pt/TiO_2 nano-composite thin films, Journal of Magnetism and Magnetic Materials 331 (2013) 187–192.

[10] S. R. Pouran, A. A. Abdul Raman, W. M. Ashri Wan Daud, Review on the application of modified iron oxides as heterogeneous catalysts in Fenton reactions, Journal of Cleaner Production, 64 (2014) 24-35.

[11] H. Mechakra, T. Sehili, M.A. Kribeche, A.A. Ayachi, S. Rossignol, C. George, Use of natural iron oxide as heterogeneous catalyst in photo-Fenton-like oxidation of chlorophenyl urea herbicide in aqueous solution: Reaction monitoring and degradation pathways, Journal of Photochemistry and Photobiology A: Chemistry, 317 (2016)140-150.

[12] E. A. Campos, D. V. B. Stockler Pinto, J. I. S. de Oliveira, E. D. C. Mattos, R. D. C. L. Dutra. Synthesis, characterization and applications of iron oxide nanoparticles – a short review, Journal of Aerospace Technology and Management, 7 (2015) 267-276.

[13] J.W. Jang , C. Du, Y. Ye, Y. Lin, X. Yao , J. Thorne, E. Liu, G. McMahon, J. Zhu, A. Javey, J. Guo & D. Wang, Enabling unassisted solar water splitting by iron oxide and silicon, Nature communications, 6 (2015) 7447.

[14] J. Tuček, K. C. Kemp, K. S. Kim, and R. Zbořil, Iron-oxide-supported nano carbon in lithium-ion batteries, medical, catalytic, and environmental applications, ACS Nano, 8 (2014) 7571-7612.

[15] R. Lebrun, A. Ross, S. A. Bender, A. Qaiumzadeh, L. Baldrati, J. Cramer, A. Brataas, R. A. Duine, M. Kläui, Tunable long-distance spin transport in a crystalline antiferromagnetic iron oxide, Nature 561(2018) 222–225.

[16] S.W. Youn, M. J. Kim, S. Yi, H. J. Ahn, K. K. Park, J. Lee, Y.-C. Lee, Effect of manganese content on the magnetic susceptibility of ferrous manganese alloys: correlation between microstructure on x-ray diffraction and size of the low-intensity area on MRI, Investigative Magnetic Resonance Imaging, 19 (2015) 76-87.

[17] M. Mozaffaria, B. Behdadfara, J. Amighiana, Preparation and characterization of manganese ferrite nanoparticles via co-precipitation method for hyperthermia, Iranian Journal of Pharmaceutical Sciences Spring, 4 (2008) 115-118.

[18] A. T. Famojuro, O Ojo, G. O. Egharevba, and M. A. Maaza, Sol-gel/hydrothermal synthesis of mixed metal oxide of titanium and zinc (tio /zno) nanocomposites through direct chemical method, Ife Journal of Science, 15 (2013) 2.

[19] R. Epherre, E. Duguet, S. Mornet, E. Pollert , S. Louguet, S. Lecommandoux, C. Schatz, G. Goglio. Manganite perovskite nanoparticles for self-controlled magnetic fluid hyperthermia: about the suitability of an aqueous combustion synthesis route. Journal of Material Chemistry, 21 (2011) 4393–4401.

[20] C.H. Ashok, K. Venkateswara Rao, C.H. Shilpa Chakra, Synthesis and characterization of MgO/TiO_2 nanocomposites. Journal of Nanotechnology, 6 (2015) 329.

[21] C.A. Eckert, R.B. Irwln, C.W. Graves, Liquid metal solvent selection: the MgO reduction reaction. Industrial & Engineering Chemistry Process Design and Development, 23 (1984) 210-217.

[22] M. Houshiar, F. Zebhi, Z. J. Razi, A. Alidoust, Z. Askari, Synthesis of cobalt ferrite ($CoFe_2O_4$) nanoparticles using combustion, coprecipitation, and precipitation methods: A comparison study of size, structural, and magnetic properties, Journal of Magnetism and Magnetic Materials, 371 (2014) 43–48.

[23] M.E. Abrishami, S.M. Hosseini, E.A. Kakhki, A. Kompany, M. Ghasemifard, Synthesis and structure of pure and Mn-doped zinc oxide nanoparticles, International Journal of Nanoscience, 9 (2010) 1928.

[24] S K Jena, D C Joshi, S Ghosh, K Dasari, S Thota, Dynamical response of localized electron hopping and dipole relaxation in $Cu_{1-x}Zn_xFe_2O_4$ magneto ceramics, Journal of Physics D: Applied Physics, 54 (2021) 425303 .

[25] C.G. Koops, On the dispersion of resistivity and dielectric constant of some semiconductors at audio frequencies. Physical Review, 83 (1951) 121–124.

[26] J. C. Papaioannoua, G. S. Patermarakis, H. S. Karayiannib, Electron hopping mechanism in hematite (a-Fe_2O_3), Journal of Physics and Chemistry of Solids 66 (2005) 839–844.

[27] N. Rezlescu, E. Rezlescu, Dielectric properties of copper containing ferrites, Physica Status Solidi 23 (1974) 575-582.